Received: 16 February 2017 | Revised: 11 August 2017 | Accepted: 6 October 2017

DOI: 10.1002/gj.3067

WILEY

RESEARCH ARTICLE

Lithospheric mantle processes beneath Kurose islet, Southwest Japan

The Cong Nguyen | Youngwoo Kil | Junghwan Seol

[1] Department of Energy and Resources Engineering, Chonnam National University, Gwangju, Korea

Correspondence
Y. Kil, Department of Energy and Reources Engineering, Chonnam National University, 77 Yongbong-ro, Buk-gu, Gwangju 500-757, Korea.
Email: ykil@jnu.ac.kr

Handling Editor: C.Manikyamba Nguyen

Upper mantle xenoliths enclosed in Cenozoic alkali basalts in Southwest Japan were found at Kurose Islet. The xenoliths consist primarily of harzburgite and minor lherzolite and exhibit a porphyroclastic texture. Trace element data showing relative depletion in light rare earth elements (REEs) and general spoon-shaped patterns suggest that xenoliths experienced depletion and slight enrichment processes. Incompatible trace element patterns for the spinel peridotite xenoliths indicate varying degrees of modification by fractional melting (from 6 to 11%). The Kurose spinel peridotites appear to have undergone melt extraction followed by an episode of cryptic mantle metasomatism. A nearby silicate melt may have been the metasomatic agent affecting spinel peridotites. The spinel peridotites originated from depths of 48 to 51 km at equilibrium temperatures ranging from 1030 to 1082 °C.

KEYWORDS

Kurose islet, lithospheric mantle, metasomatism, spinel peridotite

1 | INTRODUCTION

Ultramafic xenoliths provide valuable evidence of the chemical composition, mineralogy, and P-T conditions for the lower crust and lithospheric mantle (Chattopadhaya et al., 2017; Kaczmareck et al., 2016; MaalØe & Aoki, 1977; Nixon, 1987; Perinelli, Bosi, Andreozzi, Conte, & Armienti, 2014; Rudnick, 1992; Satsukawa, Godard, Demouchy, Michibayashi, & Ildefonse, 2017). As noted in previous studies, most examples of mantle-derived xenoliths occur in association with continental rifts or oceanic hot spots (Nixon, 1987). Mantle xenoliths from the Japanese island arc have provided information concerning composition of the lithospheric mantle in a subduction setting in which they may have specifically derived from a mantle wedge (Aoki & Fujimaki, 1982; Takahashi, 1978).

Numerous studies have addressed the lower crust and lithospheric mantle of various localities in the Southwest Japan arc (Abe, Arai, & Yurimoto, 1998; Aoki, 1987; Arai, 1978; Arai, 1994; Arai, Abe, & Hirai, 1998; Arai, Abe, Hirai, & Shimizu, 2001; Arai, Hirai, & Uto, 2000; Takahashi, 1978). Kurose islet is located in Hakata Bay, Fukuoka Prefecture, Southwest Japan, about 500 m north of Genkai Island (Figure 1). Kurose islet consists primarily of alkali basalt, which hosts abundant lithospheric mantle and lower crustal xenoliths. Kurose's xenolith-bearing alkali basalt has been mentioned and described by Arai and Hirai (1983), Hirai (1986), Abe et al. (1998), Arai et al. (2000), and Arai et al. (2001, 2007). The Kurose peridotites have not been studied in terms of their degree of partial melting, metasomatic alteration or pressure–temperature history within the lithospheric mantle.

This study reports new modal and chemical data on the Kurose islet xenoliths in order to clarify the composition and petrogenetic history of the spinel peridotites. The petrologic and geochemical data provide new constraints on partial melting, mantle metasomatism, and original crystallization depth for bodies formed within the lithospheric mantle beneath Kurose islet.

2 | TECTONIC SETTING

The Japanese island arc lies at the intersection of four major tectonic plates: the Pacific, Philippine, North American, and Eurasian Plate. The arc consists of the four big islands: Hokkaido, Honshu, Shikoku, and Kyushu. Honshu and Shikoku comprise the Southwest Japanese arc (Taira, 2001). Volcanic activity occurs in this area due to northwestward subduction of the Philippine Plate, which also formed a back-arc basin during the Neogene period. This back-arc basin generated volcanism and contributed to the shape of the Japanese arc configuration (Taira, 2001). Most xenolith-bearing alkali basalts found in Southwest Japan formed from eruptions occurring after the East Sea (Sea of Japan) opened at around 15 Ma (Arai et al., 2000). Alkali basalt localities of the Southwest Japanese arc typically cluster together spatially, but Kurose is an isolated islet far removed from other

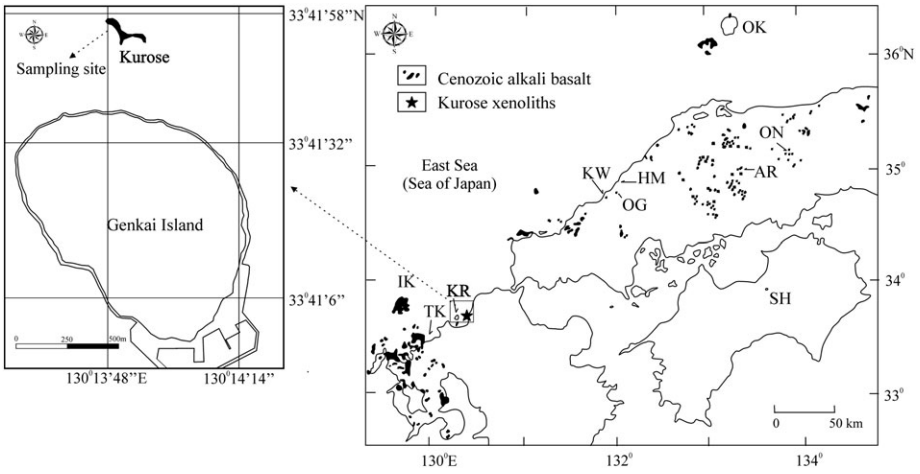

FIGURE 1 Localities of the study area and other major xenolith-bearing alkali basalts in Southwest Japanese arc. KR, Kurose, OK = Oki–Dogo, ON = On–Yama, AR = Aratoyama, HM = Hamada, OG = Noyamadake, KW = Kawashima, SH = Shingu, IK = Iki, and TK = Takashima. Map modified from Arai et al. (2001)

examples of associated magmatism. The alkali basalt of Kurose formed during the early Quaternary period and gives an absolute K-Ar age of around 1.13 ± 0.12 Ma (Uto, Hirai, & Arai, 1993). It therefore represents the youngest volcanic activity among the xenolith-bearing basalts found in Southwest Japan. Iwamori (1991) argued that asthenospheric upwelling during the Miocene period caused eruptions of intra-plate alkali basalts at Kurose and other localities. This event may have also caused mantle process that occurred in the lithospheric mantle beneath Kurose islet. According to size and shape distributions, several types of lower crustal and lithospheric mantle xenoliths occur within the Kurose alkali basalts. We collected various mantle-derived xenoliths composed of spinel peridotite, dunite, and pyroxenite as well as lower crustal xenoliths composed of granulite and granite.

3 | METHODOLOGY

Xenoliths were selected for analysis based on their appearance and lack of secondary alteration. Minerals were partly separated under a binocular microscope for petrographic characterization. Quantitative, *in-situ* analysis of major element compositions in olivine, orthopyroxene, clinopyroxene and spinel (both cores and rims) were performed using an Electron Micro Probe Analyser (EPMA, Shimadzu 1600) at Chonnam National University (CNU). All elemental analyses for minerals were carried out with a 15 kV acceleration voltage, 1 μm beam size, and 20 s peak counting time. The counting precision for EPMA measurements was ±0.5%. Ferrous and ferric ions of minerals were separated from the total iron using methods described in Droop (1987). Equilibrium temperature and pressure condition estimates were performed using the PTMafic (v.2.00) software package (Soto & Soto, 1995).

Trace element analysis of clinopyroxenes was performed using a Laser Ablation Inductively Coupled Plasma Mass Spectrometer (LA–ICP–MS) at the Korea Basic Science Institute (KBSI) operated at 10 Hz frequency, using 100 μm beam size and with a 11.39 J/cm^2 pulse energy. The percent relative standard deviation (% RSD) was within 5–10%.

Major and trace element abundances within the alkali basalt host rock were measured by X–ray Fluorescence (XRF) at the Korea Institute of Geoscience and Mineral Resources (KIGAM) and by Inductively Coupled Plasma–Mass Spectrometry (ICP–MS) at CNU. Measurement precision fell within ±15% of measured values for trace elements. The RSD of Certified Reference Material (NIST 612) is shown in Table 4.

4 | RESULTS

4.1 | Petrography

Peridotite xenoliths hosted by the alkali basalt were carefully selected from 13 hand specimens based on lack of visible alteration, including secondary alteration or other evidence of reaction with the host rock. The selected peridotites consisted mostly of olivine (50–80%) and orthopyroxene (15–45%) with minor clinopyroxene (2–6%), and accessory spinel (0.2–2.4%). Given the general lack of clinopyroxene, these samples classify as spinel peridotites. Ternary plots of modal compositions (Figure 2 with data given in Table. 1) show that 12 samples fall into the spinel harzburgite field while one sample classifies as a spinel lherzolite. The peridotites from Kurose in Southwest Japan are dominanted by intermediate lherzolite–harzburgite, whereas those from South Korea are primarily fertile spinel lherzolite (Figure 2). Mercier and Nicolas (1975) described spinel peridotites as characterized by porphyroclastic textures (Figure 3a) composed of over 50% small polygonal neoblasts appearing in thin sections.

Olivine porphyroclasts observed from Kurose peridotites are relatively large (~2 mm) and exhibit rounded to irregular shapes with kinked and bent morphologies (Figure 3b). The kinked crystals indicate a dislocational impact on crystals and cause undulose extinction features apparent in thin section. This texture arises from thermal shock during peridotite incorporation into hotter basaltic magma or from a deformation event occcurring in the lithospheric mantle after the rock formed (Tracy, 1980). Olivine neoblasts exhibit an average size of about 0.3 mm and are typically round or polygonal in shape, a morphology that creates triple junctions at grain boundaries. Within neoblasts,

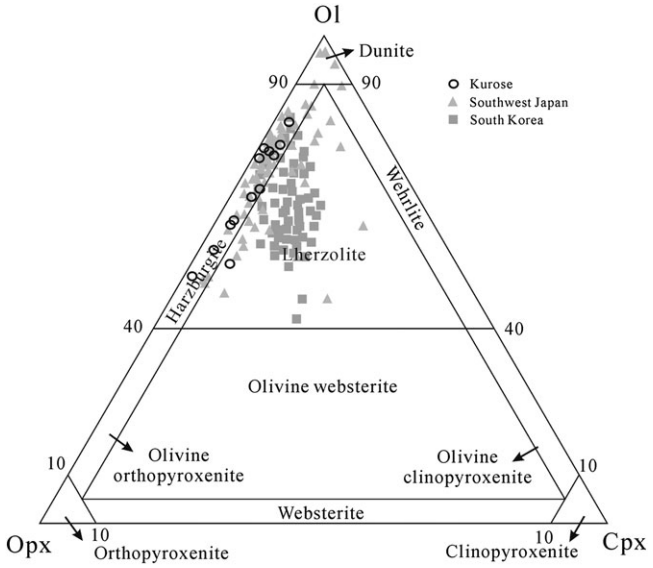

FIGURE 2 The modal composition of spinel peridotites from Kurose compares with those from Southwest Japan and South Korea. Data sources for Southwest Japan are from Abe et al. (1998), Abe, Takami, and Arai (2003), Arai et al. (2001), Goto and Arai (1987), Satsukawa et al. (2017) and those for South Korea are from Choi, Lee, Park, and Moutte (2002), Choi, Kwon, Mukasa, and Sagong (2005), Choi and Kwon (2005), Kil and Lee (2005), Kil (2006), Kil (2007), Shin, Kil, Jin and Lee (2006). Ol = olivine, Opx = orthopyroxene, Cpx = clinopyroxene

TABLE 1 Modal composition of spinel peridotites (%) from Kurose

Sample	Rock type	Ol	Opx	Cpx	Spl	Cpx/Opx
KRS 2	Spl–ha	56.17	40.32	2.75	0.76	0.07
KRS 4	Spl–ha	73.72	21.46	2.66	2.17	0.12
KRS 5	Spl–ha	79.70	15.66	2.69	1.95	0.17
KRS 11	Spl–ha	66.91	26.75	4.41	1.93	0.16
KRS 15	Spl–ha	65.10	28.72	3.79	2.40	0.13
KRS 20	Spl–ha	61.26	34.16	3.05	1.53	0.09
KRS 23	Spl–ha	73.88	24.40	1.14	0.57	0.05
KRS 26	Spl–ha	75.77	19.49	3.51	1.23	0.18
KRS 28	Spl–ha	75.83	22.38	1.61	0.19	0.07
KRS 29	Spl–ha	50.95	46.82	1.37	0.86	0.03
KRS 31	Spl–lh	53.67	39.64	6.12	0.56	0.15
KRS 32	Spl–ha	60.56	35.36	2.81	1.27	0.08
KRS 33	Spl–ha	74.22	21.45	3.22	1.11	0.15

Ol = olivine, Opx = orthopyroxene, Cpx = clinopyroxene, Spl = Spinel, Spl–ha = spinel harzburgite, Spl-lh = spinel lherzolite.

olivines with abundant sub–grain boundaries indicate recrystallization of original olivine porphyroclasts. Along with kink bands in olivine porphyroclasts, neoblasts offer evidence of deformational processes affecting the spinel peridotites at both low and high temperatures (Passchier & Trouw, 2005).

Orthopyroxenes with characteristic dark green colour occur within the porphyroclast as relatively large bodies (up to 3 mm) relative to other minerals. They typically exhibit equant or tabular morphologies and partial replacement by olivines. Orthopyroxenes also show kink bands, undulatory phenomena and exsolution textures containing thin clinopyroxene lamellae oriented within the host (Figure 3c). This texture indicates cooling of the peridotites prior to enclosure within the alkali basalt. The orthopyroxenes within the neoblasts vary in size from 0.3 to 0.5 mm and are polygonal in shape with triple junctions at their boundaries (Figure 3d). These neoblasts possibly originated from progressive recrystallization along the margins of porphyroclasts.

Clinopyroxenes were less abundant and often concentrated in small clusters within the spinel peridotites. These rarely occur in porphyroclasts but were present in void spaces between olivines and orthopyroxenes as neoblast grains (Figure 3e). Most of the clinopyroxenes were subhedral or irregular in shape, exhibited a range of grain sizes (0.3–0.5 mm) with both straight and serrated boundaries. Occasionally, clinopyroxenes occurred as small inclusions within the olivine or orthopyroxene host indicating possible recrystallization processes.

Spinels in the peridotites occurred as small dark brown grains (0.1–0.4 mm) with irregular, vermicular or weakly elongated morphologies (Figure 3f). They are dispersed within neoblasts of porphyroclastic peridotites and also occur as intergrowths in orthopyroxene or clinopyroxene hosts. The absence of hydrous minerals such as phlogopite and amphibole in the spinel peridotites indicates equilibration under dry conditions.

4.2 | Mineral chemistry

4.2.1 | Major elements

Table 2 shows representative major elements for predominant spinel peridotite minerals. Whole-rock peridotites and alkali basalt compositions are shown in Table 3. The whole-rock peridotite compositions were calculated by mass balance of mineral compositions and modal abundances. Olivines exhibit a range of Fo values (100*Mg/[Mg + Fe^{2+}]) from 89.3 to 90.4, which resemble those reported for so-called abyssal peridotites (Dick & Fisher, 1984), which originate from beneath the ocean crust. Olivine NiO and MnO contents range from 0.15 to 0.26 wt.% and 0.10 to 0.21 wt.%, respectively. These values fell within range of similar values reported for spinel peridotites from various global localities (Nixon, 1987). In addition, olivines exhibited very low concentrations of Al_2O_3 (< 0.1 wt.%) and CaO (<0.15 wt.%).

Orthopyroxenes categorize as enstatite given their compositional ranges of $Wo_{1.5–1.8}En_{88.7–89.8}Fs_{8.5–9.4}$. The range of Mg# [Mg/(Mg + Fe^{2+})], averaging around 0.91, was relatively narrow but similar to that observed in olivines. The Al_2O_3, Cr_2O_3, and CaO abundances ranged from 2.15 to 3.82 wt.%, 0.46 to 0.67 wt.%, and 0.74 to 0.93 wt.%, respectively.

Clinopyroxenes categorized as Cr–diopside given their $Wo_{45.5–46.9}En_{48.9–50.6}Fs_{3.6–4.1}$ ranges. Clinopyroxene Mg# varied from 0.92 to 0.94, values that were relatively higher than that of coexisting olivines and orthopyroxenes. The Al_2O_3 and Cr_2O_3 abundances ranged from 2.16 to 4.08 wt.% and 0.59 to 1.12 wt.%, respectively. Clinopyroxenes exhibited relatively high CaO, which ranged from 20.19 to 22.49 wt.%.

Spinels categorize as Cr–spinel with Cr_2O_3 and Al_2O_3 contents ranging from 18.36 to 37.89 wt.% and 29.93 to 50.72 wt.%,

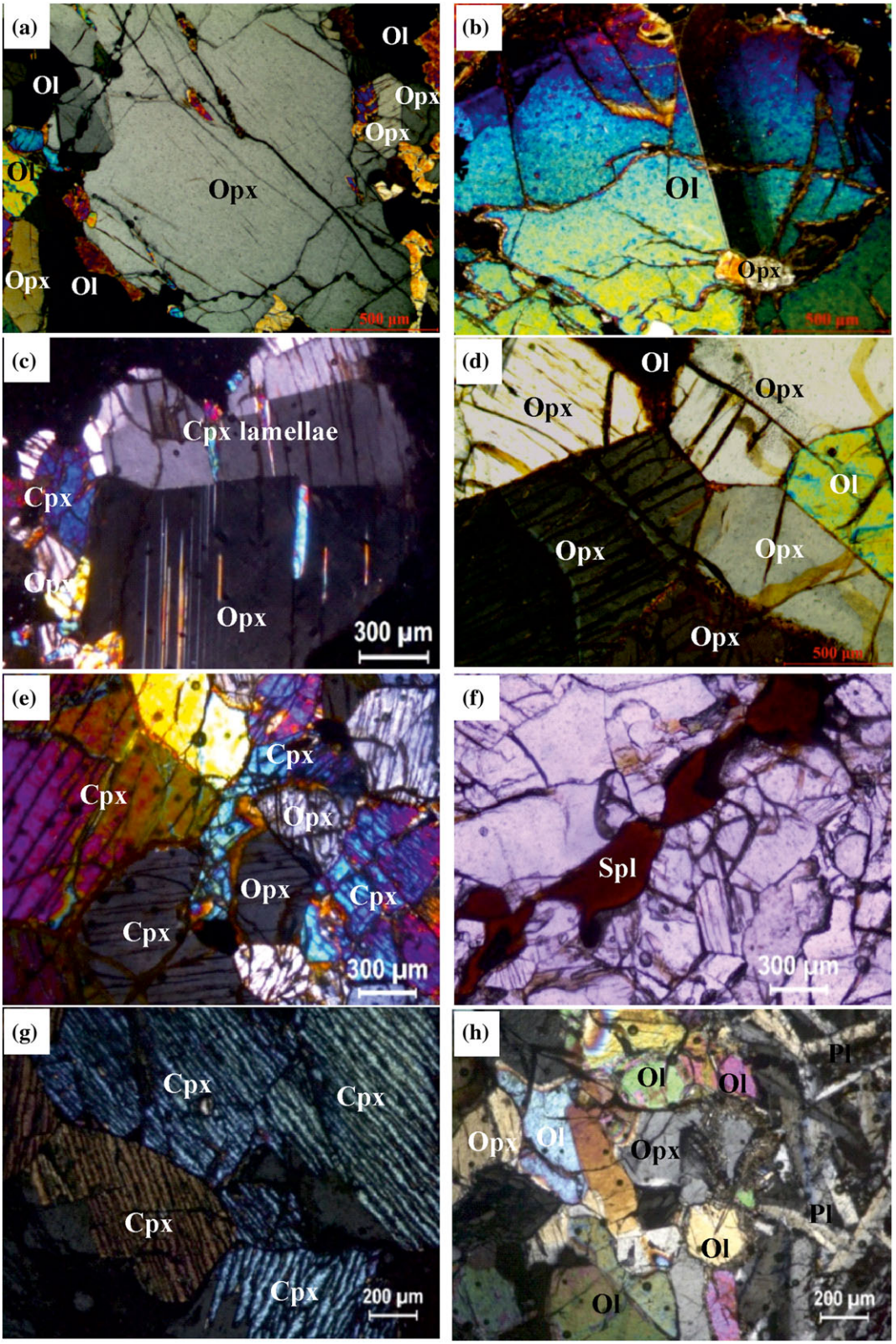

FIGURE 3 Thin section photomicrographs of xenoliths from Kurose. (**a**) Porphyroclastic texture (Krs 5). (**b**) Large kinked olivine porphyroclast (Krs 2). (**c**) Orthopyroxene porphyroclast with exsolution lamellae of clinopyroxenes (Krs 28). (**d**) Orthopyroxene neoblast display triple junction on boundaries (Krs 3). (**e**) Subhedral clinopyroxenes in neoblast (Krs 4). (**f**) Elongated spinel (Krs 2). (**g**) Clinopyroxenes in pyroxenite vein. (**h**) Infiltration of magma into the spinel peridotite (KRS 4) (See Table 2 for explanation of mineral abbreviations) [Colour figure can be viewed at wileyonlinelibrary.com]

respectively. Values for Cr# [Cr/(Cr + Fe^{3+}+Al)] ranged from 0.20 to 0.46, similar to those measured from abyssal peridotites which contain Cr# < 0.55 (Dick & Fisher, 1984).

4.2.2 | Trace elements in clinopyroxene

Petrogenetic processes in the mantle tend to strongly influence trace elements leading to their lower abundance in the lithospheric mantle.

TABLE 2 Representative major element compositions (wt.%) of olivine, orthopyroxene, clinopyroxene, and spinel in spinel peridotites from Kurose

Sample	KRS 2–Harzburgite				KRS 4–Harzburgite				KRS 5–Harzburgite			
Mineral	Ol	Opx	Cpx	Sp	Ol	Opx	Cpx	Sp	Ol	Opx	Cpx	Sp
SiO_2	40.19	56.04	55.25	0.02	41.05	56.91	55.56	0.03	40.61	55.28	55.37	0.01
TiO_2	–	0.28	0.01	0.29	0.01	0.16	0.01	0.53	–	0.15	0.02	0.24
Al_2O_3	0.02	3.67	3.11	49.18	0.03	2.59	2.60	33.67	0.01	3.80	2.58	47.79
Cr_2O_3	0.02	0.53	0.65	20.15	0.04	0.60	0.88	33.85	–	0.59	0.89	20.86
FeO	9.85	5.97	2.35	12.56	9.55	5.75	2.26	15.40	9.91	6.01	2.23	12.82
NiO	0.17	0.09	0.01	0.17	0.26	0.04	0.03	0.12	0.22	0.07	0.03	0.19
MnO	0.18	0.14	0.16	0.16	0.12	0.08	0.09	0.25	0.14	0.15	0.09	0.13
MgO	49.14	32.68	16.50	17.90	49.54	33.76	16.82	15.50	48.78	33.17	16.89	17.50
CaO	0.08	0.78	22.04	–	0.06	0.81	21.90	0.01	0.07	0.84	21.93	–
Na_2O	–	–	0.30	0.02	–	0.02	0.38	–	–	0.01	0.38	–
K_2O	–	–	0.01	–	–	–	0.01	–	–	0.01	–	–
Total	99.66	100.17	100.39	100.45	100.66	100.71	100.54	99.36	99.73	100.08	100.41	99.53
Sample	KRS 11–Harzburgite				KRS 15–Harzburgite				KRS 20–Harzburgite			
Mineral	Ol	Opx	Cpx	Sp	Ol	Opx	Cpx	Sp	Ol	Opx	Cpx	Sp
SiO_2	41.02	56.14	55.20	0.03	40.61	56.05	54.93	0.03	40.81	56.07	54.29	0.08
TiO_2	0.07	0.21	–	0.20	–	0.07	0.01	0.35	–	0.17	0.02	0.17
Al_2O_3	0.01	3.22	3.17	44.20	–	3.68	3.30	47.95	0.03	3.60	3.82	50.72
Cr_2O_3	–	0.53	0.84	24.60	0.01	0.57	0.59	20.86	0.02	0.46	0.91	18.85
FeO	9.63	5.82	2.18	13.38	9.90	6.07	2.43	12.58	9.90	6.13	2.43	12.20
NiO	0.20	0.03	0.02	0.09	0.24	0.07	0.04	0.17	0.24	0.06	0.03	0.22
MnO	0.15	0.13	0.03	0.17	0.13	0.14	0.10	0.13	0.12	0.09	0.06	0.16
MgO	49.38	33.51	16.83	17.05	49.09	32.99	16.71	17.72	48.94	32.74	16.17	18.06
CaO	0.06	0.76	21.83	–	0.08	0.86	21.95	–	0.08	0.89	21.52	0.02
Na_2O	–	–	0.24	–	–	–	0.28	–	–	–	0.26	–
K_2O	0.01	–	0.01	0.01	0.01	0.01	–	–	–	–	0.01	–
Total	100.51	100.35	100.35	99.73	100.05	100.51	100.35	99.79	100.15	100.21	99.52	100.48
Sample	KRS 23–Harzburgite				KRS 26–Harzburgite				KRS 28–Harzburgite			
Mineral	Ol	Opx	Cpx	Sp	Ol	Opx	Cpx	Sp	Ol	Opx	Cpx	Sp
SiO_2	41.64	55.96	54.56	0.04	40.67	56.58	54.22	0.05	40.94	56.70	55.03	0.03
TiO_2	–	0.30	0.02	0.41	0.10	0.20	–	0.42	0.16	0.09	0.02	0.98
Al_2O_3	–	3.82	3.42	45.67	–	3.28	3.23	42.86	–	2.49	2.76	30.08
Cr_2O_3	0.03	0.64	0.74	22.95	0.05	0.55	0.83	24.73	–	0.67	1.12	37.34
FeO	10.03	6.06	2.43	13.06	10.23	6.04	2.34	14.18	9.45	5.58	2.12	15.07
NiO	0.16	0.01	0.03	0.17	0.18	0.05	0.03	0.16	0.23	0.08	0.02	0.12
MnO	0.21	0.15	0.10	0.16	0.14	0.14	0.08	0.19	0.16	0.18	0.10	0.24
MgO	48.30	32.82	17.01	17.52	49.17	32.75	16.69	16.91	49.93	32.78	16.54	15.15
CaO	0.09	0.86	21.51	0.01	0.06	0.81	21.36	–	0.08	0.93	20.84	–
Na_2O	0.03	0.05	0.48	0.03	–	0.02	0.30	–	–	0.04	0.60	–
K_2O	0.02	–	0.02	–	–	–	0.02	–	0.01	0.02	0.01	0.01
Total	100.50	100.67	100.32	100.01	100.60	100.40	99.10	99.51	100.95	99.54	99.17	99.02
Sample	KRS 31– Lherzolite				KRS 32–Harzburgite				KRS 33– Harzburgite			
Mineral	Ol	Opx	Cpx	Sp	Ol	Opx	Cpx	Sp	Ol	Opx	Cpx	Sp
SiO_2	41.38	57.27	54.65	0.04	41.69	56.54	54.08	0.03	41.13	56.21	54.35	0.05
TiO_2	–	0.20	0.02	0.78	–	0.18	0.01	0.30	0.02	0.23	0.01	0.43
Al_2O_3	–	2.15	2.16	30.12	0.10	3.43	3.58	47.87	0.02	3.28	3.06	43.92
Cr_2O_3	0.03	0.53	0.67	37.72	–	0.55	0.75	21.06	–	0.61	0.74	23.44
FeO	9.95	5.94	2.26	16.02	10.08	6.05	2.35	12.86	10.22	6.05	2.43	14.31
NiO	0.23	0.10	0.03	0.07	–	0.08	0.03	0.17	0.20	0.06	0.04	0.15
MnO	0.16	0.14	0.11	0.26	0.10	0.18	0.11	0.13	0.18	0.22	0.07	0.17

(Continues)

TABLE 2 (Continued)

Sample	KRS 31– Lherzolite				KRS 32–Harzburgite				KRS 33– Harzburgite			
Mineral	Ol	Opx	Cpx	Sp	Ol	Opx	Cpx	Sp	Ol	Opx	Cpx	Sp
MgO	48.52	33.60	17.73	14.45	48.43	32.56	16.97	17.85	48.08	32.95	16.73	17.03
CaO	0.05	0.79	22.25	–	0.15	0.86	21.82	0.01	0.09	0.80	22.09	–
Na_2O	0.01	–	0.33	–	0.04	0.02	0.30	0.01	–	–	0.30	–
K_2O	0.02	–	0.02	0.01	0.04	0.01	0.01	0.01	0.03	–	0.04	0.01
Total	100.36	100.71	100.22	99.46	100.63	100.45	100.01	100.29	99.96	100.40	99.85	99.51

All values were performed by EPMA. Ol = olivine, Opx = orthopyroxene, Cpx = clinopyroxene, Sp = spinel.

TABLE 3 Whole-rock composition (wt%) of spinel peridotites and alkali basalt from Kurose

Whole rock	KRS 2	KRS 4	KRS 5	KRS 11	KRS 15	KRS 20	KRS 23	KRS 26	KRS 28	KRS 29	KRS 31	KRS 32	KRS 33	Alkali basalt
SiO_2	46.72	43.66	42.59	44.70	44.51	45.74	44.80	43.54	44.39	48.15	48.01	46.51	44.30	48.63
TiO_2	0.11	0.05	0.03	0.11	0.03	0.06	0.07	0.12	0.14	0.03	0.08	0.07	0.07	2.64
Al_2O_3	1.95	1.38	1.61	1.86	2.33	2.14	1.23	1.28	0.66	2.11	1.15	1.97	1.30	15.16
Cr_2O_3	0.40	0.92	0.52	0.65	0.69	0.48	0.32	0.48	0.24	0.44	0.48	0.48	0.42	–
FeO	8.11	8.61	9.17	8.32	8.57	8.40	8.94	9.14	8.41	8.19	7.89	8.42	9.11	11.84
NiO	0.13	0.20	0.19	0.14	0.18	0.17	0.12	0.15	0.19	0.11	0.16	0.03	0.16	–
MnO	0.17	0.11	0.14	0.14	0.13	0.11	0.19	0.14	0.16	0.14	0.15	0.13	0.19	0.19
MgO	41.44	44.26	44.97	42.87	42.42	41.87	43.76	44.19	45.17	40.03	40.34	41.31	43.47	7.20
CaO	0.96	0.80	0.77	1.20	1.12	1.01	0.52	0.96	0.61	0.77	1.70	1.01	0.95	8.40
Na_2O	0.01	0.01	0.01	0.01	0.01	0.01	0.04	0.01	0.02	0.02	0.03	0.04	0.01	3.97
K_2O	–	–	–	–	–	–	0.02	–	0.01	0.01	0.01	0.03	0.02	0.84
P_2O_5	–	–	–	–	–	–	–	–	–	–	–	–	–	0.38
Total	100.00	100.00	100.00	100.00	100.00	100.00	100.00	100.00	100.00	100.00	100.00	100.00	100.00	99.25

Wt% of spinel peridotites was calculated by mass balance method. Wt% of alkali basalt was determined by XRF.

Relative abundances of trace elements can therefore indicate compositional variation in the lithospheric mantle compositions and/or the relative intensity of mantle processes. In the spinel peridotites considered here, clinopyroxene was the principal host of trace elements and a likely source for nearly all REEs measured in whole-rock powders. This assumption is based on the fact that clinopyroxene's M2–site is larger than that of coexisting minerals (Nagasawa, Schreiber, & Morris, 1980; Stosch, 1982).

Table 4 shows representative trace element compositions of clinopyroxene in spinel peridotites from Kurose. Primitive–normalized REE plots from clinopyroxenes cluster into distinctive subsets of depleted and spoon-shaped patterns. The depleted subset exhibits a slight depletion in the light REEs, compared with the middle and heavy REEs (Figure 4a). Values for (Sm/Yb)n and (La/Yb)n ranged from 0.4–0.9 and 0.1–0.5, respectively. The so-called spoon-shaped patterns exhibit a strong depletion in the heavy to middle REEs with (Sm/Yb)n ratios of 0.1–0.2, followed by slight enrichment in the light REEs (Figure 4b) and relatively uniform (flat) La to Nd concentrations. The following discussion interprets the potential petrogenetic implications of these patterns.

5 | DISCUSSION

5.1 | Petrogenesis and partial melting

The absence of plagioclase and garnet in harzburgites and clinopyroxene-poor lherzolites from Kurose indicates that the peridotites have been equilibrated in the spinel peridotite field (Arai, 1994). As shown in spinel Cr# versus Mg# variation diagrams (Figure 5a) and Cr# in spinel versus Fo in olivine (Figure 5b) diagrams, most samples fall within a field associated with abyssal peridotite. Kurose peridotites from Southwest Japan originated from the back-arc side of Japan arcs, while the peridotites from South Korea, which plotted close to the Fertile MORB Mantle (FMM; Figure 5b), were formed at the Eurasian continental margin. Abe et al. (1998) suggested that the peridotites from the Japan arc derive from the same source as the abyssal peridotite but may have evolved through a different process. The peridotite compositions beneath the Japan arcs are modified by regional mantle wedge metasomatism; the process happening in Kurose was caused by a metasomatic agent, which will be discussed in a later section.

Kurose spinel peridotites exhibit very low clinopyroxene modal compositions (mostly <4 vol.%, except for in sample KRS31) relative to primitive mantle material highlighting a significant depletion in this mineral. Clinopyroxene/orthopyroxene ratios decrease with clinopyroxene's abundance indicating partial melting of clinopyroxene solution (Figure 6a). Inverse relations between Al_2O_3 and MgO in the clinopyroxene (Figure 6b) also indicate mantle depletion caused by partial melting (Norman, 1998). A positive correlation between the Cr# in spinels and that observed in coexisting clinopyroxenes (Figure 6c) as well as inverse relations between Cr# and Mg# contained in the same host (Figure 6d) provide further evidence of partial melting of spinel peridotites (Dick & Bullen, 1984). The

TABLE 4 Representative trace element compositions (ppm) of clinopyroxene in spinel peridotites and host rock from Kurose

Element	Krs2	Krs 4	Krs 5	Krs 11	Krs 15	Krs 20	Krs 23	Krs 26	Krs 31	Krs 32	Krs 33	Host rock Alkali basalt	NIST 612 Average (n = 10)	RSD
Rock type	Sp-ha	Sp-ha	Sp-ha	Sp-ha	Sp-ha	Sp-ha	Sp-ha	Sp-ha	Sp-lh	Sp-ha	Sp-ha			(%)
P	134	163	92	198	171	220	141	114	74	90	118	–	-	–
Sc	71.4	88.0	77.5	100.0	81.8	84.8	74.3	78.2	82.4	69.5	73.8	42458	31.0	15.1
Ti	1292	952	839	942	1116	1234	1186	739	863	881	955	503	–	–
V	184	210	178	238	251	259	212	193	159	183	196	3861	34.3	4.3
Cr	2916	5789	5339	4364	4181	4755	5584	3828	3998	3878	3870	–	37.9	7.1
Mn	406	508	459	507	548	541	419	419	466	488	437	106	34.7	5.8
Co	20.5	27.8	24.3	24.9	29.7	28.3	22.7	21.4	23.1	25.3	23.3	230	30.1	9.9
Ni	294	400	370	379	449	408	313	298	320	372	340	437	33.6	15.0
Cu	0.91	4.27	2.96	23.58	7.77	5.67	2.19	2.21	3.84	3.27	5.44	176	23.9	14.9
Zn	7.61	11.4	10.0	9.60	12.7	12.7	7.95	8.61	9.02	10.1	8.77	3529	34.3	6.4
Rb	–	0.17	0.15	0.13	0.09	0.13	–	0.19	0.03	0.02	-	1531	28.8	11.4
Sr	4.31	22.7	19.2	4.03	3.18	0.96	3.36	11.9	22.6	3.92	13.3	42.5	71.4	4.2
Y	8.95	5.98	5.32	8.78	8.00	9.51	8.33	6.61	5.96	7.65	6.48	417	33.8	7.1
Zr	1.24	3.68	2.82	1.01	0.14	0.41	2.04	1.12	2.40	0.21	1.78	415	42.4	7.6
Nb	0.09	0.26	0.09	0.07	0.07	0.03	0.02	0.07	0.06	0.03	0.02	10.7	54.2	15.2
Mo	0.09	0.04	–	–	0.13	0.22	–	-	-	0.05	0.12	1.13	36.1	5.0
Cd	0.94	1.70	0.53	0.49	2.53	0.52	0.39	1.90	0.49	0.62	0.45	1.42	23.6	9.8
Sb	0.04	0.08	0.05	0.06	0.08	0.10	0.03	–	0.03	0.03	–	1.59	40.4	15.0
Cs	–	0.01	0.01	–	0.01	–	0.01	0.01	–	–	0.02	1571	40.4	9.4
Ba	0.02	0.09	0.05	0.11	0.10	0.49	0.09	0.28	0.08	0.10	0.04	58.1	36.3	4.3
La	0.12	0.67	0.55	0.13	0.12	0.06	0.05	0.33	0.55	0.12	0.37	105	33.7	2.5
Ce	0.32	2.07	1.65	0.47	0.21	0.16	0.26	0.99	1.67	0.31	1.48	13.1	38.3	5.1
Pr	0.07	0.36	0.34	0.06	0.02	0.02	0.07	0.12	0.26	0.03	0.30	56.1	33.8	4.9
Nd	0.70	2.46	2.04	0.32	0.10	0.17	0.59	0.62	1.53	0.16	1.59	11.9	32.1	7.6
Sm	0.49	0.77	0.58	0.28	0.15	0.31	0.34	0.27	0.59	0.16	0.40	5.42	34.0	7.0
Eu	0.23	0.26	0.29	0.11	0.11	0.14	0.19	0.11	0.23	0.08	0.22	13.7	31.6	6.2
Gd	1.17	1.21	1.05	0.70	0.72	0.85	1.13	0.60	0.79	0.63	0.78	1.71	32.2	7.6
Tb	0.27	0.21	0.17	0.21	0.20	0.26	0.24	0.16	0.19	0.17	0.19	9.17	32.2	4.5
Dy	2.34	1.45	1.40	1.86	1.92	2.33	2.20	1.46	1.39	1.96	1.58	1.76	33.4	9.5
Ho	0.52	0.34	0.31	0.47	0.50	0.56	0.51	0.38	0.33	0.42	0.40	4.52	34.1	6.2
Er	1.51	1.03	0.88	1.58	1.70	1.73	1.72	1.20	1.07	1.43	1.17	0.72	34.1	6.5
Tm	0.24	0.14	0.14	0.27	0.25	0.25	0.22	0.19	0.16	0.22	0.14	4.18	33.2	6.1
Yb	1.37	0.91	0.82	1.57	1.53	1.79	1.48	1.32	1.10	1.40	1.09	0.71	35.3	9.6
Lu	0.18	0.14	0.15	0.26	0.22	0.25	0.19	0.16	0.14	0.20	0.14	9.37	32.9	6.4
Hf	0.19	0.17	0.15	0.09	0.04	0.12	0.16	0.09	0.15	0.05	0.09	42.0	34.0	4.8
Ta	0.01	0.03	0.02	0.01	0.02	0.02	–	0.02	0.08	0.01	0.08	9.45	40.1	5.5
Pb	0.69	0.76	0.38	0.13	0.16	2.53	0.05	0.53	0.40	0.30	0.07	8.68	33.8	3.3
Th	0.04	0.07	0.04	0.03	0.06	0.02	0.02	0.03	0.07	0.04	0.03	3.47	34.4	5.2
U	0.02	0.05	0.09	0.03	0.03	0.04	–	0.04	0.02	0.01	0.02	–	33.2	6.9

Values of spinel peridotites and host rock were performed by LA-ICP-MS and ICP-MS, respectively. Rock types: Sp-ha, spinel harzburgite; Sp-lh, spinel lherzolite. n: times of measurement

correlations of modal and whole-rock compositions (Figure 6e,f) provide the affirmation for this process. The depletion in most incompatible elements of clinopyroxene is an important factor for observing melt extraction. Therefore, REE concentrations in clinopyroxene were used to constrain the degree of melting. Slight REE depletion indicates that the spinel peridotites had experienced low degrees of partial melting (Figure 7b). Partial melting can occur as either batch or fractional melting, which were assumed in interpreting melt process related to incompatible element concentrations observed in the residual solid.

REE concentrations from Kurose clinopyroxenes were compared with theoretical values calculated for clinopyroxenes from mantle residual melts having experienced various degrees of batch and fractional melting. The results were obtained using equations from

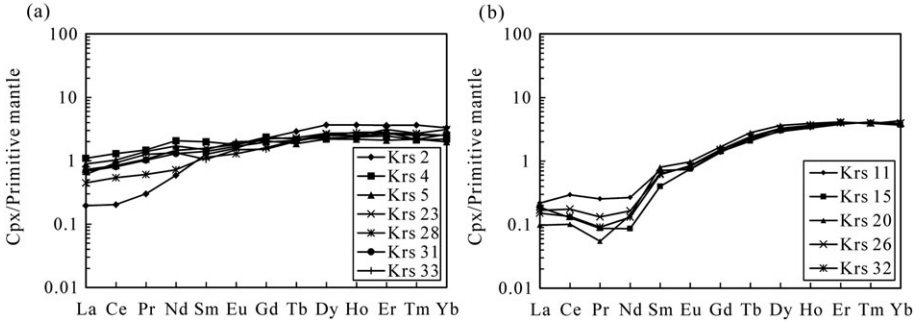

FIGURE 4 Primitive mantle-normalized rare earth element patterns of clinopyroxenes in spinel peridotites from Kurose. (**a**) Depletion-shape type. (**b**) Spoon-shape type. Primitive mantle values are from Hofmann (1988)

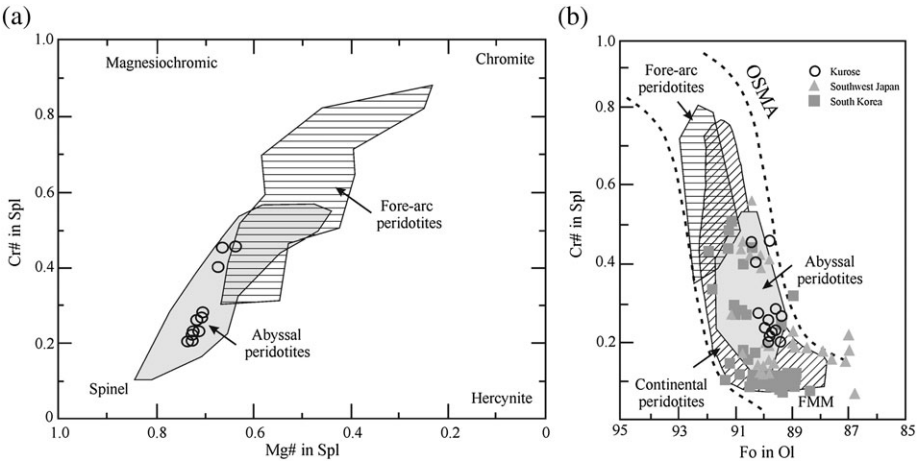

FIGURE 5 (**a**) Plots of Cr# vs. Mg# in spinel of spinel peridotites from Kurose. (**b**) Plots of Fo in olivine vs. Cr# in spinel of Kurose peridotites compared with those from Southwest Japan and South Korea. Data sources for Southwest Japan are from Abe et al. (2003), Arai et al. (2000), Arai et al. (2001), Goto and Arai (1987), Satsukawa et al. (2017), Umino and Yoshizawa (1996) and those for South Korea from Choi et al. (2002), Choi et al. (2005), Choi and Kwon (2005), Choi, Jwa, and Lee (2001), Lee (1996), Kil (2006, 2007), Kil, Shin, and Ko (2007); Kil, Shin, and Yun (2008). Field of abyssal peridotite are from Dick and Bullen (1984) and Dick (1989); field of fore-arc peridotite are from Ishii, Robinson, Maekawa, and Fiske (1992) and field of continental peridotites are from Arai (1994). OSMA = olivine-spinel mantle array and FMM = Fertile MORB Mantle (Arai, 1994)

Norman (1998) with assumed initial bulk compositions values (C_0) for primitive mantle from Hofmann (1988). In the batch melting model (Figure 7a), large degrees of melting (10–90%) are not compatible with the observed degree of partial melting (mostly less than 40%) for peridotites (Arai, 1994). A degree of melting of less than 11% is adequate to generate the observed spinel peridotites through fractional melting (Figure 7b).

The highly incompatible LREEs are unreliable proxies in clinopyroxene for calculating the degree of melting because metasomatic processes can augment La, Ce, and Pr concentrations. We selected two less incompatible elements, Y and Yb (in clinopyroxene), for detailed calculation of fractional melting degrees. When compared with values from primitive mantle after fractional melting, (Y)n versus (Yb)n variation diagrams (Figure 8) indicate that 6 to 11% melting of a source could produce the Kurose samples. The limited range of melting agrees with that estimated by many physical models, which show relatively limited melt extraction from the mantle (Menzies, Kempton, & Dungan, 1985; O'Nions & McKenzie, 1988) and indicate relatively low degrees of partial melting in production of abyssal peridotites (<10%; Johnson, Dick, & Shimizu, 1990).

5.2 | Cryptic metasomatism

As noted by previous studies, mantle metasomatism commonly occurs within the upper mantle (Bailey, 1970; Bailey, 1982; Bailey, 1987; Bodinier, Vasseur, Vernieres, & Dupuy, 1990; Dobosi, Downes, Embey-Isztin, & Jenner, 2003; Menzies, Rogers, Tindle, & Hawkesworth, 1987; Roden & Murthy, 1985; Varela, Clocchiatti, Massare, & Schiano, 1998). Xenolith localities throughout the Japanese arc offer evidence of these processes, which exert a major influence on the geochemistry of the lithospheric mantle in the area (Abe et al., 1998). Three types of metasomatism can occur: patent metasomatism (modal metasomatism), cryptic metasomatism (Dawson, 1984), and Fe-Ti metasomatism (Wilshire, 1987).

Patent metasomatism is characterized by the appearance of hydrous minerals such as amphibole or phlogopite, and/or anhydrous minerals such as zircon, apatite, rutile, and crichtonite-series minerals. Cryptic metasomatism meanwhile appears as enrichment in several incompatible trace elements, such as K, Rb, Sr, Ba, REE, and P, without introduction of new minerals (Dawson, 1984). Finally, Fe-Ti metasomatism appears as enrichment in Fe, Ti, and other components in

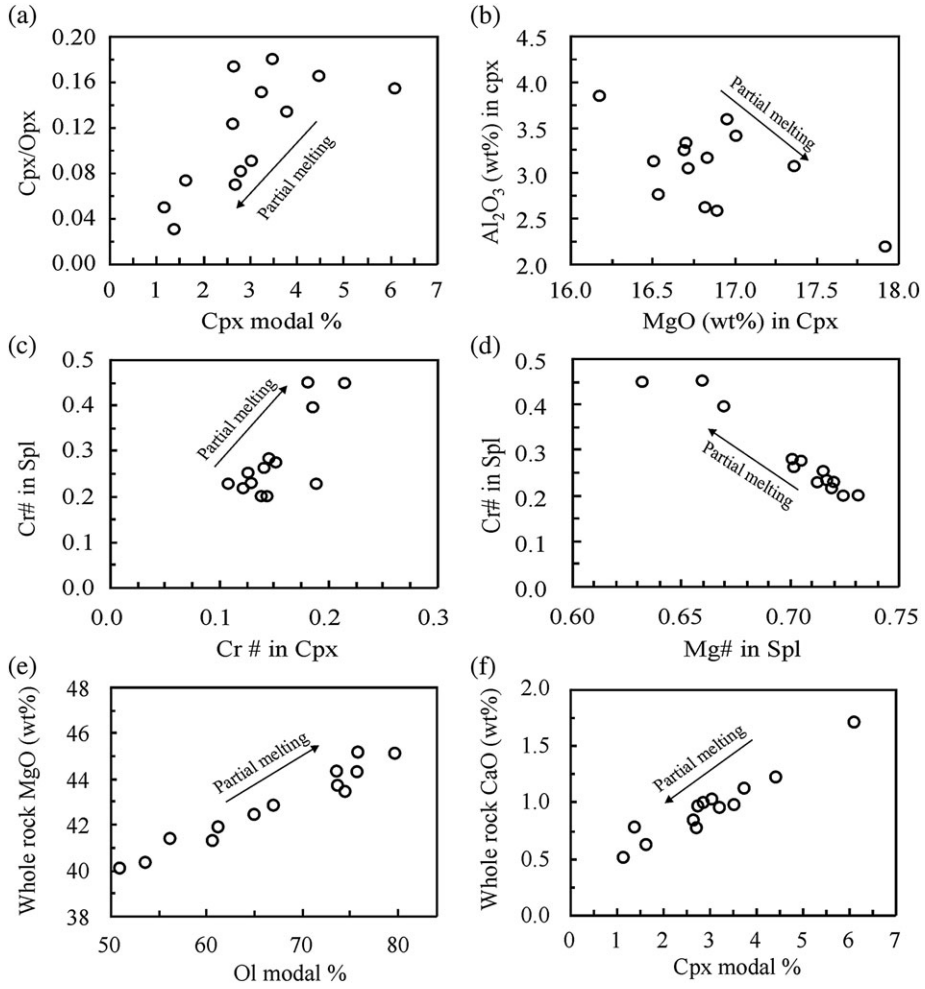

FIGURE 6 Diagrams of various characteristics of spinel peridotites from Kurose: (**a**) Cpx modal vs. Cpx/Opx modal ratio. (**b**) MgO vs. Al_2O_3 in Cpx. (**c**) Cr# in Cpx vs. Cr# in Spl. (**d**) mg# vs. Cr# in Spl. (**e**) Olivine modal vs. whole rock MgO. (**f**) Cpx modal vs. whole rock CaO. Ol = olivine, Opx = orthopyroxene, Cpx = clinopyroxene, Spl = spinel

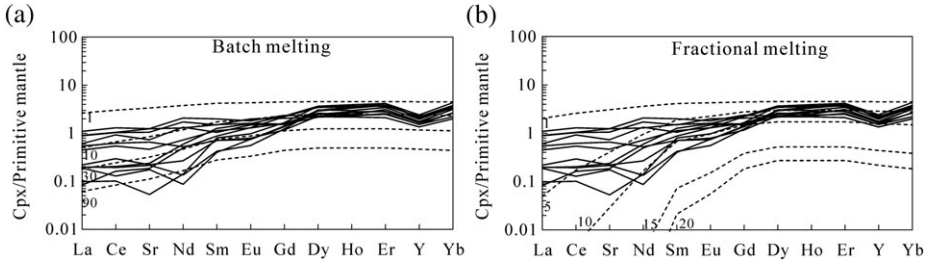

FIGURE 7 Primitive mantle–normalized REEs in clinopyroxenes from Kurose compared to clinopyroxene in primitive mantle having undergone partial melting. (**a**) Batch melting model (between 1 and 90%) and (**b**) fractional melting model (between 1 and 20%). Primitive mantle values are from Hofmann (1988)

peridotite wall rock caused by interaction with mafic magma, here represented by pyroxenites with or without hydrous phases (Wilshire, 1987; Wilshire & Jackson, 1975; Wilshire & Shervais, 1975). Fe-Ti metasomatism is also associated with crosscutting dikes, which contain Cr–diopside pyroxenites, Au–augite pyroxenites, garnet and spinel bearing pyroxenites, and/or hydrous phases such as amphibole (±Fe-Ti phlogopite) bearing Al-augite pyroxenites (Wilshire, 1987).

The absence of new minerals within the Kurose spinel peridotite xenoliths indicates that they did not experience patent metasomatism. Spinel peridotite xenoliths from Kurose are also relatively homogeneous in thin section, offering no evidence of Fe-Ti metasomatism. Although no hydrous minerals occur within the xenoliths, the depletion of middle and heavy REEs and the slight enrichment of LREEs (spoon-shaped pattern) in clinopyroxenes indicates that the spinel peridotites have experienced cryptic metasomatism. The enrichment of several incompatible elements, especially HFSEs, relative to primitive mantle, also indicate this type of metasomatism (Dawson, 1984).

The metasomatic agents including H_2O-CO_2 fluid, carbonatite melt, and silicate melt were investigated to further understand cryptic metasomatism under the Kurose islet. The absence of evidence for

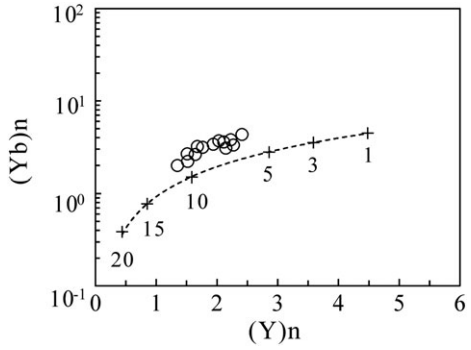

FIGURE 8 Comparison of fractional melting model for (Y)n and (Yb)n contents of clinopyroxene in spinel peridotites from Kurose. The spinel peridotites from Kurose were depleted by 6 ~ 11% fractional melting

patent metasomatism suggests that H_2O–CO_2 fluids were not major metasomatic agents because these fluids would have precipitated hydrous minerals during reaction with xenoliths (Roden & Murthy, 1985). Furthermore, fluids are preferentially partitioned into the melt phase such that the melt may be considered as an agent. We therefore investigated silicate and carbonatite melt agents.

Infiltration of a carbonatite melt into a peridotite body usually forms apatite, causes P enrichment in mantle host rock composition, and generates negative HFSE anomalies (Ionov, Prikhod'ko, & O'Reilly, 1995; Rudnick, McDonough, & Chappell, 1993). The absence of apatite/calcite, negative HFSE anomalies, (e.g., Ti, Hf, Th, U, and Ta) and the positive Ba anomalies (Figure 9) indicate that the carbonatite

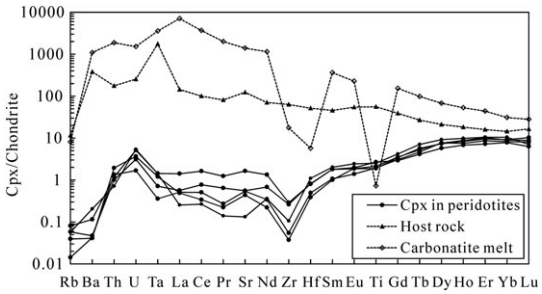

FIGURE 9 Comparison of chondrite–normalized incompatible elements in clinopyroxene of spinel peridotites for those in chondrite–normalized host rock (alkali basalt) and carbonatite melt (Bizimis et al., 2003). From left to right in order of increasing compatibility. Chondrite values are from Sun and McDonough (1989)

melt did not modify the spinel peridotites (Bizimis, Salters, & Dawson, 2003; Coltorti, Beccaluva, Bonadiman, & Salvinil., Siena., F., 2000; Green & Wallace, 1988; Ionov et al., 1995; Rudnick et al., 1993). As a result, a silicate melt is likely to have caused the cryptic metasomatism taking place within the lithospheric mantle. Low (La/Yb)n and (Zr/Sm)n relative to Ti/Eu and (Ti/Eu)n (Figures 10a,b) in spinel peridotites also offer evidence of silicate metasomatism (Coltorti et al., 2000; Coltorti, Bonadiman, Hinton, Siena, & Upton, 1999). Enrichment in highly incompatible elements (e.g., Th and U) also suggests melt—rock interactions (Bodinier, Menzies, Shimizu, Frey, & McPherson, 2004).

Figure 9 shows that chondrite–normalized incompatible element patterns in the host rock do not match those observed for clinopyroxene, especially the negative U and Th anomalies. This indicates that the host rock is not the metasomatic agent. A thin vein of Cr-diopside pyroxenite (Figure 3g) found in the peridotite xenoliths (usually referred to as composite peridotite) offers physical evidence of melt-rock interactions. The veins formed from interaction between spinel peridotites and a Cr-rich melt as the melt migrated through fractures and reequilibrated with the wall rock (Litasov, Foley, & Litasov, 2000). Verniéres, Godard, & Bodinier, J. –L., 1997 described this "percolation" process as one that led to enrichment of elements more incompatible than Ce (e.g., La, Ta, Th, and U). The silicate melt causing the percolation may have similarly infiltrated peridotites to precipitate clinopyroxene as reaction rims on olivines (Figure 3h). Cryptic metasomatism occurring within the lithospheric mantle may thus arise from infiltration of a silicate melt enriched in Th, U, Ta, and LREEs. Silicate melt-peridotite interactions may have also enriched these elements.

Previous studies by Arai et al. (2000) and Arai et al. (2001) concluded that Kurose xenoliths did not experience metasomatism. Along these lines, we suggest that cryptic metasomatism occurred only sparsely beneath Kurose islet and its evidence appears in a few of our samples. Iwamori (1991) suggested that asthenospheric upwelling during the Miocene caused emplacement of within-plate alkali basalts and metasomatism of the lithospheric mantle beneath the Japanese arc. This study however offers no evidence of the relation between silicate metasomatism and the postulated upwelling.

5.3 | Equilibrium pressure and temperature conditions

Well-defined grain boundaries, absence of reaction rims, and homogeneous chemical compositions between cores and rims of individual

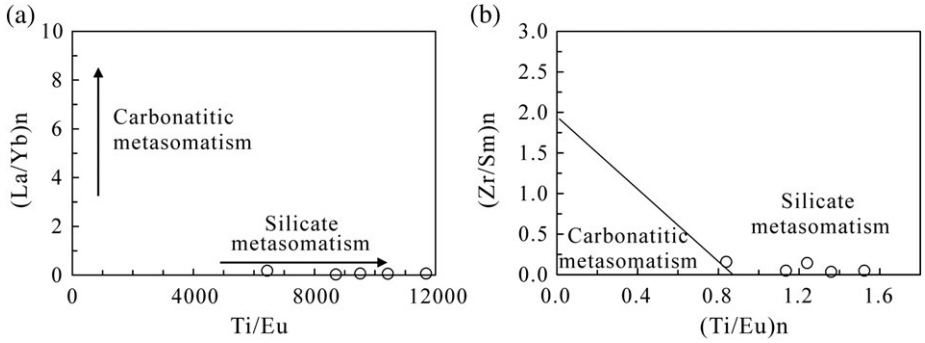

FIGURE 10 **(a)** Ti/Eu vs. (La/Yb)n ratios of clinopyroxenes in spinel peridotites from Kurose, trends of silicate and carbonatite metasomatism are from Coltorti et al. (1999). **(b)** (Ti/Eu)n versus $(La/Yb)_n$ ratios, fields of silicate and carbonatite metasomatism are from Coltorti et al. (2000)

minerals indicate that spinel peridotites enjoyed petrologic equilibrium prior to incorporation into the alkali basalt host rock (Kil, 2002). Coexisting minerals wthin the peridotites can therefore be used for geothermobarometric calculations. Geothermometers of two–pyroxene (Bertrand & Mercier, 1985; Brey & Köhler, 1990; Wood & Banno, 1973), single–orthopyroxene (Brey & Köhler, 1990), and olivine–orthopyroxene–spinel (Witt-Eickschen & Seck, 1991) were used to calculate equilibrium temperatures at an assumed pressure of 15 kb. Olivine–clinopyroxene (Köhler & Brey, 1990), spinel (O'neil, 1981), and single–clinopyroxene (Mercier, 1980) geobarameters meanwhile provided equilibrium pressures. Major element compositions of minerals provided equilibrium temperature and pressure estimates for comparison but showed no significant variation between core and rim (Table 5). Due to its relatively independent assumptions concerning pressure, the Brey and Köhler (1990) geothermometer offers robust temperature estimates based on calcium exchange reactions between orthopyroxene and clinopyroxene. Equilibrium temperature estimates for the Kurose spinel peridotite range from 1030 to 1082 °C. These correspond well with the range of equilibrium temperatures estimated for the spinel peridotite field (900–1100 °C; Gasparik, 1984).

The equilibrium temperatures obtained from this study agree with those reported in Arai et al. (2001), which range from 1000 to 1100 °C as estimated by methods suggested in Wells (1977). Equilibrium temperatures for Kurose spinel peridotites are lower than those estimated for similar bodies from other Japanese arc localities such as Takashima (1000–1150°°C; Arai et al., 2001), Noyamadake (approximately 1200 °C; Arai & Hirai, 1983), and Fukue–Jima (1070–1200 °C; Umino & Yoshizawa, 1996). These data indicate lateral heterogeneity of the lithospheric mantle underlying the Japan arc.

Köhler and Brey (1990) developed a geobarometer to determine equilibrium pressures for Kurose spinel peridotites (Table 5). The temperature uncertainty of the Brey and Köhler (1990) geothermometer is ±15°°C, corresponding to ±2–3 kb uncertainty (Soto & Soto, 1995). O'Reilly, Chen, Griffin, and Ryan (1997) suggest that the ±50 °C uncertainty of the geothermometer correspond to ±8 kb uncertainty for the Köhler and Brey (1990) geobarometer. If this temperature uncertainty is accepted, it renders the geobarometer inaccurate. In addition, estimated equilibrium pressures for spinel peridotite, which varied over a wide range of 9–26 kb, are unreliable because the geobarometer depends on temperature variations (Kil, 2002). Current geobarometers cannot accurately determine equilibrium pressure for spinel peridotite (Kil, 2002; Medaris, Ackerman, Jelínek, & Magna, 2014). O'neil (1981) geobarometer, based on Cr content of spinel, only provides an upper limit of the equilibrium pressure for Kurose spinel peridotites. Extraction depths of mantle xenoliths can be deduced from the results of geothermometry and geothermal gradient (Medaris et al., 2014). Coupled with heat flow data, the Brey and Köhler (1990) geothermometer can also provide an estimate for the depth at which Kurose spinel peridotie xenoliths formed. The areas surrounding Kurose exhibit approximate heat flow values of 70 mW/m^2 (Tanaka, Yamano, Yano, & Sasada, 2004). Methods by Sclater, Jaupart, and Galson (1980) provide estimates for the geothermal gradient. Crustal

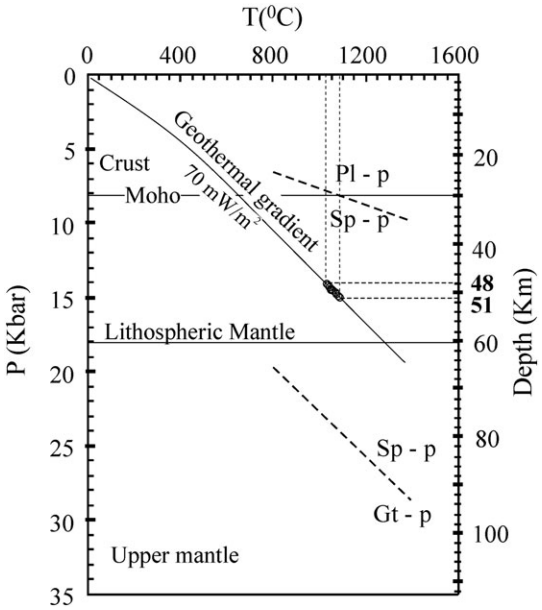

FIGURE 11 Extraction depths of spinel peridotites from Kurose deduced from temperature condition. Temperatures was estimated using the Brey and Köhler (1990) geothermometer. The crust thickness is 30 km (Salah & Zhao, 2004). Average lithosphere thickness is 60 km (Yoshizawa et al., 2010). Heat flow is 70 mW/m^2 (Tanaka et al., 2004). Geothermal gradient curve deduced from heat flow by method of Sclater et al. (1980). Boundary of Pl-p (plagioclase peridotite) and Sp-p (spinel peridotite) is from O'neil (1981) and Gasparik (1987) and boundary of Sp-p and Gt-p (garnet peridotite) is from Köhler and Brey (1990)

TABLE 5 Temperature–pressure data for Kurose spinel peridotite xenoliths

Sample Rock type	Krs 2 Sp–ha	Krs 4 Sp–ha	Krs 5 Sp–ha	Krs 11 Sp–ha	Krs 15 Sp–ha	Krs 20 Sp–ha	Krs 23 Sp–ha	Krs 26 Sp–ha	Krs 28 Sp–ha	Krs 31 Sp–lh	Krs 32 Sp–ha	Krs 33 Sp–ha
T_{BK} (°C) at 15 kb	1052	1060	1051	1068	1071	1078	1046	1065	1082	1030	1044	1047
T_{BM} (°C) at 15 kb	1212	1227	1231	1255	1258	1255	1259	1253	1291	1252	1251	1203
T_{WB} (°C) at 15 kb	1057	1069	1075	1088	1088	1081	1091	1083	1029	1085	1087	1056
$T_{ca\text{-}in\_opx}$ (°C) at 15 kb	986	1002	1014	990	1025	1029	1025	994	1108	1006	1017	998
T_{WS} (°C) at 15 kb	892	964	936	873	935	884	950	946	1045	930	897	918
P_{KB} (kb)	15	20	14	24	15	15	12	26	16	20	9	11
P_O (maximum) (kb)	25	30	26	26	26	25	26	27	31	31	26	26
PM (kb)	13	12	13	13	13	13	13	13	13	12	13	13

T = geothermometer, P = geobarometer, T_{BK} = Brey and Köhler (1990), T_{BM} = Bertrand and Mercier (1985), T_{WB} = Wood and Banno (1973), $T_{Ca\text{-}in\text{-}Opx}$ = Brey and Köhler (1990), T_{WS} = Witt-Eickschen and Seck (1991); P_{KB} = Köhler and Brey (1990), P_O = O'neil (1981), P_M = Mercier (1980).

thickness (Moho depth) estimated from seismograms and waveform data reaches about 30 km along the coast of southwestern Japan and within the East Sea (Salah & Zhao, 2004). Original depths beneath Kurose at which the spinel peridotites formed may thus vary from 48 to 51 km (Figure 11). Xenoliths may occur in the middle-lower part of the lithospheric mantle as estimated from the Moho depth (30 km) and the average lithospheric thickness of the East Sea (about 60 ± 10 km; Yoshizawa, Mizake, & Yomogida, 2010).

6 | CONCLUSIONS

Lithospheric mantle xenoliths beneath Kurose islet entrapped by alkali basalt exhibit porphyroclastic textures and consist of primarily harzburgite and subordinate lherzolite. The Fo in olivine along with the Cr# and Mg# in spinel and clinopyroxene of the peridotites resemble that measured from abyssal peridotites indicating a shared parental magma source.

A scarcity of clinopyroxene in the spinel peridotites and general compositional variation indicate partial melting by melt extraction occuring within the lithospheric mantle. Correlation between REEs, especially Yb and Y, suggest that spinel peridotites have undergone 6–11% fractional melting.

Primitive–normalized REEs in clinopyroxenes exhibit a spoon-shaped pattern indicating that spinel peridotites have experienced partial melting and subsequent cryptic metasomatism, which caused light REE enrichment. Silicate melts were the likely metasomatic agent.

According to Brey and Köhler (1990) geothermometers, equilibrium temperatures of the spinel peridotites range from 1030 to 1082 °C. Along with pressure (Mercier, 1980) and heat flow data beneath Kurose, these temperatures suggest that the peridotite developed at 48–51 km depth.

ACKNOWLEDGEMENTS

We are grateful to Dr. Takashi Sano of National Museum of Nature and Science, Tokyo, for supporting to collect the samples from Kurose. This work was supported by the Energy Efficiency and Resources of the Korea Institute of Energy Technology Evaluation and Planning (KETEP) grant funded by the Korea Government Ministry of Trade, Industry and Energy (20152510101980).

ORCID

Youngwoo Kil http://orcid.org/0000-0003-0799-9884

REFERENCES

Abe, N., Arai, S., & Yurimoto, H. (1998). Geochemical characteristics of the uppermost mantle beneath the Japan island arcs: Implications for upper mantle evolution. *Physics of the Earth and Planetary Interiors*, *107*, 233–248.

Abe, N., Takami, M., & Arai, S. (2003). Petrological feature of spinel lherzolite xenolith from Oki-Dogo Island: An implication for variety of the upper mantle peridotite beneath southwestern Japan. *Island Arc*, *12*, 219–232.

Aoki, K. (1987). Japanese Island arc: xenoliths in alkali basalts, high–alumina basalts, and calc–alkaline andesites and dacites. In P. H. Nixon (Ed.), *Mantle xenoliths* (pp. 319–333). New York: John Wiley and Sons.

Aoki, K., & Fujimaki, H. (1982). Petrology and geochemistry of calc-alkaline andesite of presumed upper mantle origin from Itinome–gata, Japan. *American Mineralogist*, *67*, 1–13.

Arai, S. (1978). Chromian spinel lamellae in olivine from the Iwanai–dake peridotite mass, Hokkaido, Japan. *Earth and Planetary Science Letters*, *39*, 267–273.

Arai, S. (1994). Characterization of spinel peridotites by olivine–spinel compositional relationships: Review and interpretation. *Chemical Geology*, *113*, 191–204.

Arai, S., & Hirai, H. (1983). Petrographical notes on deep–seated and related rock: 1. Mantle peridotites from Kurose and Noyamadake alkali basalts, southwestern Japan. *Annual Report of the Institute Geoscience University of Tsukuba*, *9*, 65–67.

Arai, S., Abe, N., & Hirai, H. (1998). Petrological characteristics of the sub–arc mantle: An overview on petrology of peridotite xenoliths from the Japan arcs. *Trends in Mineral*, *2*, 40–45.

Arai, S., Hirai, H., & Uto, K. (2000). Mantle peridotite xenoliths from the Southwest Japan arc: A model for the sub–arc upper mantle structure and composition of the Western Pacific rim. *Journal of Mineralogical and Petrological Sciences*, *95*, 9–23.

Arai, S., Abe, N., Hirai, H., & Shimizu, Y. (2001). Geological, petrographical and petrological characteristics of ultramafic xenoliths in Kurose and Takashima, northern Kyusu, southwestern Japan. *The Science reports of the Kanazawa University*, *46*, 9–38.

Arai, S., Abe, N., & Ishimaru, S. (2007). Mantle peridotites from the Western Pacific. *Gondwana Research*, *11*, 180–199.

Bailey, D. K. (1970). Volatile flux, heat focusing and the generation of magma. *Geological Journal Special Issue*, *2*, 177–186.

Bailey, D. K. (1982). Mantle metasomatism–continuing chemical change within the earth. *Nature*, *296*, 525–530.

Bailey, D. K. (1987). Mantle metasomatism–perspective and prospect. *Geological Society of London, Special Publication*, *30*, 1–13.

Bertrand, P., & Mercier, J. C. C. (1985). The mutual solubility of coexisting ortho–and clinopyroxene: Toward an absolute geothermometer for the natural system? *Earth and Planetary Science Letters*, *76*, 109–122.

Bizimis, M., Salters, V. J. M., & Dawson, J. B. (2003). The brevity of carbonatite sources in the mantle: Evidence from Hf isotopes. *Contributions to Mineralogy and Petrology*, *145*, 281–300.

Bodinier, J. L., Vasseur, G., Vernieres, J., & Dupuy, C. F. (1990). Mechanism of mantle metasomatism: Geochemical evidence from the lherz orogenic peridotite. *Journal of Petrology*, *31*, 597–628.

Bodinier, J. L., Menzies, M. A., Shimizu, N., Frey, F. A., & McPherson, E. (2004). Silicate, hydrous and carbonate metasomatism at Lherz, France: Contemporaneous derivatives of silicate melt – harzburgite reaction. *Journal of Petrology*, *45*, 299–320.

Brey, G. P., & Köhler, T. (1990). Geothermobarometry in four–phase lherzolites II. New thermobarometers, and practical assessment of existing thermobarometers. *Journal of Petrology*, *31*, 1353–1378.

Chattopadhaya, S., Ghosh, B., Morishita, T., Nandy, S., Tamura, A., & Bandyopadhyay, D. (2017). Reaction microtextures in entrapped xenoliths in alkali basalts from the Deccan large igneous province, India: Implications to the origin and evolution. *Journal of Asian Earth Sciences*, *138*, 291–305.

Choi, S. H., & Kwon, S.-T. (2005). Mineral chemistry of spinel peridotite xenoliths from Baengnyeong Island, South Korea, and its implications for the paleogeotherm of the uppermost mantle. *Island Arc*, *14*, 236–253.

Choi, S. H., Jwa, Y.-J., & Lee, H. Y. (2001). Geothermal gradient of the upper mantle beneath Jeju Island, Korea: Evidence from mantle xenoliths. *Island Arc*, *10*, 175–193.

Choi, S. H., Lee, J. I., Park, C. H., & Moutte, J. (2002). Geochemistry of peridotite xenoliths in alkali basalts from Jeju Island, Korea. *Island Arc*, *11*, 221–235.

Choi, S. H., Kwon, S.-T., Mukasa, S. B., & Sagong, H. (2005). Sr-Nd-Pb isotope and trace element systematics of mantle xenoliths from Late Cenozoic alkaline lavas, South Korea. *Chemical Geology*, *221*, 40–64.

Coltorti, M., Bonadiman, C., Hinton, R. W., Siena, F., & Upton, B. G. J. (1999). Carbonatite metasomatism of the oceanic upper mantle: Evidence from clinopyroxenes and glasses in ultramafic xenoliths of Grande Comore, Indian Ocean. *Journal of Petrology*, *40*, 133–165.

Coltorti, M., Beccaluva, L., Bonadiman, C., & Salvinil., Siena., F. (2000). Glasses in mantle xenoliths as geochemical indicators of metasomatic agents. *Earth and Planetary Science Letters*, *183*, 303–320.

Dawson, J. B. (1984). Constrasting types of upper mantle metasomatism? In J. Kornprobst (Ed.), *Kimberlites II* (pp. 289–294). Amsterdam: Elsevier.

Dick, H. J. B. (1989). Abyssal peridotites, very slow spreading ridges and ocean ridge magmatism. In A. D. Saunders, & M. J. Norry (Eds.), *Magmatism in the ocean Basins* (pp. 71–105). Blackwell: Geological Society of London Special Publications **42**.

Dick, H. J. B., & Bullen, T. (1984). Chromian spinel as a petrogenetic indicator in abyssal and alpine–type peridotites and spatially associated lavas. *Contributions to Mineralogy and Petrology*, *86*, 54–76.

Dick, H. J. B., & Fisher, R. L. (1984). Mineralogic studies of the residues of mantle melting: abyssal and alpine–type peridotites. In J. Kornprobst (Ed.), *The Third International Kimberlite Conference* (pp. 295–308). Amsterdam: Elsevier.

Dobosi, G., Downes, H., Embey-Isztin, A., & Jenner, G. A. (2003). Origin of megacrysts and pyroxenite xenoliths from the Pliocene alkali basalts of the Pannonian Basin (Hungary). *Neues Jahrbuch für Mineralogie Abhandlungen/Journal of Mineralogy and Geochemistry*, *178*, 217–237.

Droop, G. T. R. (1987). A general equation for estimating Fe^{3+} concentration in ferromagnesian silicates and oxides from microprobe analyses, using stoichiometric criteria. *Mineralogical Magazine*, *51*, 431–435.

Gasparik, T. (1984). Two-pyroxene thermobarometry with new experimental data in the system CaO-MgO-Al_2O_3-SiO_2. *Contributions to Mineralogy and Petrology*, *87*, 87–97.

Gasparik, T. (1987). Two–pyroxene thermobarometry with new experimental data in the system CaO–MgO–Al_2O_3–SiO_2. *Contributions to Mineralogy and Petrology*, *87*, 87–97.

Goto, K., & Arai, S. (1987). Petrology of peridotite xenoliths in lamprophyre from Shingu, southwestern Japan: Implications for origin of Fe-rich mantle peridotites. *Mineralogy and Petrology*, *37*, 137–155.

Green, D. H., & Wallace, M. E. (1988). Mantle metasomatism by ephemeral carbonatite melts. *Nature*, *336*, 459–462.

Hirai, H. (1986). *Petrology of ultramafic xenoliths from Noyamadake and Kurose, southwestern Japan*. Ph.D thesis, University of Tsukuba, 1–181.

Hofmann, A. W. (1988). Chemical differentiation of the earth: The relationship between mantle, continental crust, and oceanic crust. *Earth and Planetary Science Letters*, *90*, 297–314.

Ionov, D. A., Prikhod'ko, V. S., & O'Reilly, S. Y. (1995). Peridotite xenoliths in alkaline basalts from the Sikhote–Alin, southeastern Siberia, Russia: Trace–element signatures of mantle beneath a convergent continental margin. *Chemical Geology*, *120*, 275–294.

Ishii, T., Robinson, P. T., Maekawa, H., & Fiske, R. (1992). Petrological studies of peridotites from diapiric serpentinite seamounts in the Izu–Mariana fore-arc, Leg 125. In P. Fryer, J. A. Pearce, & L. B. Stokking (Eds.), *Proceedings of the Ocean Drilling Program* (Vol. 125, *Scientific Results, College Station: Texas, USA*) (pp. 445–485).

Iwamori, H. (1991). Zonal structure of Cenozoic basalts related to mantle upwelling in southwest Japan. *Journal of Geophysical Research*, *96*, 6157–6170.

Johnson, K. T., Dick, H. J. B., & Shimizu, N. (1990). Melting in the oceanic upper mantle: An ion microprobe study of diopsides in abyssal peridotites. *Journal of Geophysical Research*, *95*, 2661–2678.

Kaczmareck, M. A., Bodinier, J. L., Bosch, D., Tommasi, A., Dautria, J. M., & Kechid, S. A. (2016). Metasomatized Mantle Xenoliths as a Record of the Lithospheric Mantle Evolution of the Nothenrn Edge of the Ahaggar Swell, in Teria (Algeria). *Journal of Petrology*, *57*, 345–382.

Kil, Y. W. (2002). Mantle evolution associated with the Rio Grande Rift: Geochemistry and geothermobarometry of upper mantle xenoliths. Ph.D thesis, Colorado School of Mines, Golden, 1–160.

Kil, Y. (2006). Characteristics of subcontinental lithospheric mantle beneath Baegryeong Island, Korea: Spinel peridotite xenoliths. *Island Arc*, *15*, 269–282.

Kil, Y. (2007). Geochemistry and petrogenesis of spinel lherzolite xenoliths from Boeun, Korea. *Journal of Asian Earth Sciences*, *29*, 29–40.

Kil, Y., & Lee, S.-H. (2005). Geochemical characteristics of clinopyroxenes in the upper mantle rocks under the Baegryeong island and the Boeun. *Journal of the Mineralogical Society of Korea*, *18*, 61–72.

Kil, Y., Shin, H. J., & Ko, B. K. (2007). Magma pathway of alkali volcanic rocks in Goseong, Gangwon-do, Korea. *Journal of the Mineralogical Society of Korea*, *16*, 196–207.

Kil, Y., Shin, H. J., & Yun, S. H. (2008). Geochemical characteristics of mineral phases in the mantle xenoliths from Sunheul-ri, Jeju island. *Journal of the Mineralogical Society of Korea*, *21*(4), 373–382.

Köhler, T., & Brey, G. P. (1990). Calcium exchange between olivine and clinopyroxene calibrated as a geothermobarometer for natural peridotites from 2 to 60 kb with applications. *Geochimica et Cosmochimica Acta*, *54*, 2375–2388.

Lee, H. Y. (1996). Petrochemical study of mantle xenoliths in alkali basalts from South Korea: P/T regime of the upper mantle. *International Geology Review*, *38*, 320–335.

Litasov, K. D., Foley, S. F., & Litasov, Y. D. (2000). Magmatic modification and metasomatism of the subcontinental mantle beneath the Vitim volcanic field East Siberia: Evidence from trace element data on pyroxenite and peridotite xenoliths from Miocene picrobasalt. *Lithos*, *54*, 83–114.

MaalØe, S., & Aoki, K. (1977). The major element composition of upper mantle estimated from the composition of lherzolites. *Contributions to Mineralogy and Petrology*, *63*, 161–173.

Medaris, L. G. Jr., Ackerman, L., Jelínek, E., & Magna, T. (2014). Depletion, cryptic metasomatism, and modal metasomatism of central European lithospheric mantle: Evidence from elemental and Li isotope compositions of spinel peridotite xenoliths, Kozákov volcano, Czech Republic. *International Journal of Earth Sciences (Geol Rundsch)*, *104*, 1925–1956.

Menzies, M., Kempton, P., & Dungan, M. (1985). Interaction of continental lithosphere and asthenospheric melts below the Geronimo volcanic field, Arizona, USA. *Journal of Petrology*, *26*(3), 663–693.

Menzies, M., Rogers, N., Tindle, A., & Hawkesworth, C. (1987). Metasomatic and enrichment processes in lithospheric peridotites, an effect of asthenosphere-lithosphere interaction. In A. Menzies, & C. Hawkesworth (Eds.), *Mantle metasomatism* (pp. 313–361). London: Academic press.

Mercier, J. C. (1980). Single–pyroxene thermobarometry. *Tectonic Physics*, *70*, 1–37.

Mercier, J. C., & Nicolas, A. (1975). Texture and fabrics of upper mantle peridotites as illustrated by xenoliths from basalts. *Journal of Petrology*, *16*, 454–487.

Nagasawa, H., Schreiber, H. D., & Morris, R. V. (1980). Experimental mineral/liquid partition coefficient of the rare earth elements (REE), Sc and Sr for perovskite, spinel and melilite. *Earth and Planetary Science Letters*, *46*, 431–437.

Nixon, P. H. (Ed.) (1987). *Mantle xenoliths* (pp. 1–844). New York: John Wiley and Sons.

Norman, M. D. (1998). Melting and metasomatism in the continental lithosphere: Laser ablation ICPMS analysis of minerals in spinel lherzolites from eastern Australia. *Contributions to Mineralogy and Petrology*, *130*, 240–255.

O'neil, H. S. C. (1981). The transition between spinel lherzolite and garnet lherzolite, and its use as a geobarometer. *Contributions to Mineralogy and Petrology*, *77*, 185–194.

O'Nions, R. K., & McKenzie, D. P. (1988). Melting and continent generation. *Earth and Planetary Science Letters*, *90*, 449–456.

O'Reilly, S. Y., Chen, D., Griffin, W. L., & Ryan, C. G. (1997). Minor elements in olivine from spinel lherzolite xenoliths: Implications for thermobarometry. *Mineralogical Magazine*, *61*, 257–269.

Passchier, C. W., & Trouw, R. A. J. (2005). *Microtectonics* (pp. 1–366). Berlin, New York: Springer.

Perinelli, C., Bosi, F., Andreozzi, G. B., Conte, A. M., & Armienti, P. (2014). Geothermometric study of Cr-rich spinels of peridotite mantle xenoliths from northern Victoria land (Antarctica). *American Mineralogist*, *99*, 839–846.

Roden, M. F., & Murthy, V. R. (1985). Mantle metasomatism. *Annual Review of Earth and Planetary Sciences*, *13*, 269–296.

Rudnick, R. L. (1992). Xenoliths–samples of the lower continental crust. In D. Fountain, R. Arculus, & R. W. Kay (Eds.), *Continental lower crust* (pp. 269–316). Amsterdam: Elsevier.

Rudnick, R. L., McDonough, W. F., & Chappell, B. W. (1993). Carbonatite metasomatism in the northern Tanzanian mantle: Petrographic and geochemical characteristics. *Earth and Planetary Science Letters*, *114*, 463–475.

Salah, M. K., & Zhao, D. (2004). Mapping the crustal thickness in southwest Japan using Moho reflected waves. *Physical of the Earth and Planetary Interiors*, *141*, 79–94.

Satsukawa, T., Godard, M., Demouchy, S., Michibayashi, K., & Ildefonse, B. (2017). Chemical interactions in the subduction factory: New insights from an in situ trace element and hydrogen study of the Ichinomegata and Oki-Dogo mantle xenoliths (Japan). *Geochimica et Cosmochimica Acta*, *208*, 234–267.

Sclater, J. G., Jaupart, C., & Galson, D. (1980). The heat flow through oceanic and continental crust and the heat loss of the earth. *Reviews of Geophysics and Space Physics*, *18*, 269–311.

Shin, H.-J., Kil, Y., Jin, M.-S., & Lee, S.-H. (2006). Petrological study on upper mantle xenoliths from Asan and Pyongtaek area. *Journal of the Geological Society of Korea*, *42*, 95–113.

Soto, J. I., & Soto, V. M. (1995). PTMafic (v.2.0): Software package for thermometry, barometry, and activity calculations in mafic rocks using an IBM or compatible computer. *Computers and Geosciences*, *21*, 619–652.

Stosch, H. G. (1982). Rare earth element partitioning between minerals from anhydrous spinel peridotite xenoliths. *Geochemical et Cosmochimica Acta*, *46*, 793–811.

Sun, S. S., & McDonough, W. F. (1989). Chemical and isotopic systematics of oceanic basalt: implications for mantle composition and processes. In A. D. Saunders, & M. J. Norry (Eds.), *Magmatism in ocean basins* (pp. 313–345). Blackwell: Geological Society London Special Publications 42.

Taira, A. (2001). Tectonic evolution of the Japanese island arc system. *Annual Review of Earth and Planetary Sciences*, *29*, 109–134.

Takahashi, E. (1978). Petrologic model of the crust and upper mantle of the Japanese island arcs. *Bulletin Volcanologique*, *41*, 529–547.

Tanaka, A., Yamano, M., Yano, Y., & Sasada, M. (2004). Geothermal gradient and heat flow data in and around Japan (I): Appraisal of heat flow from geothermal gradient data. *Earth, Planets and Space*, *56*, 1191–1194.

Tracy, R. J. (1980). Petrology and genetic significance of an ultramafic xenolith suite from Tahiti. *Earth and Planetary Science Letters*, *48*, 80–96.

Umino, S., & Yoshizawa, E. (1996). Petrology of ultramafic xenoliths from Kishyuku Lava, Fukue-jima, Southwest Japan. *Contributions to Mineralogy and Petrology*, *124*, 154–166.

Uto, K., Hirai, H., & Arai, S. (1993). K–Ar ages for quaternary alkali basalts from Kurose, Fukuoka prefecture and Kufune, Yamaguchi prefecture Southwest Japan. *Bulletin of the Geological Survey of Japan*, *44*, 693–698.

Varela, M. E., Clocchiatti, R., Massare, D., & Schiano, P. (1998). Metasomatism in subcontinental mantle beneath Northern Patagonia (Rio Negro Province), Argentina: Evidence from silica-rich melt iclusions. *Mineralogy and Petrology*, *62*, 103–121.

Verniéres, J., Godard, M., & Bodinier, J. –L. (1997). A plate model for the simulation of trace element fractionation during partialmelting and magmas transport in the Earth's upper mantle. *Journal of Geophysical Research*, *102*, 24,771–24,784.

Wells, P. R. A. (1977). Pyroxene thermometry in simple and complex systems. *Contributions to Mineralogy and Petrology*, *62*, 129–139.

Wilshire, H. G. (1987). A model of metasomatism. In: *Mantle metasomatism and alkaline magmatism*. Morris EM, Pasteris JD. (eds). *Geological Society of America Special Papers*, *215*, 47–60.

Wilshire, H. G., & Jackson, E. D. (1975). Problems in determining mantle geotherms from pyroxene compositions of ultramafic rocks. *Journal of Geology*, *83*, 313–329.

Wilshire, H. G., & Shervais, J. W. (1975). Al-augite and Cr-diopside ultramafic xenoliths in basaltic rocks from western United States; structure and texture relationships. *Physics and Chemistry of the Earth*, *9*, 257–272.

Witt-Eickschen, G., & Seck, H. A. (1991). Solubility of Ca and Al in orthopyroxene from spinel peridotite: An improved version of an empirical geothermometer. *Contributions to Mineralogy and Petrology*, *106*, 431–439.

Wood, B. J., & Banno, S. (1973). Garnet–orthopyroxene and orthopyroxene–clinopyroxene relationships in simple and complex systems. *Contributions to Mineralogy and Petrology*, *42*, 109–124.

Yoshizawa, K., Mizake, K., & Yomogida, K. (2010). 3D upper mantle structure beneath Japan and its surrounding region from inter-station dispersion measurements of surface waves. *Physics of the Planetary Interiors*, *183*, 4–19.

How to cite this article: Nguyen TC, Kil Y, Seol J. Lithospheric mantle processes beneath Kurose islet, Southwest Japan. *Geological Journal*. 2018;53:2301–2314. https://doi.org/10.1002/gj.3067